Astronomy & Astrophysics manuscript no. lyafdf˙astro˙ph
February 16, 2007

Lyα emission in high-redshift galaxies ⋆

C. Tapken[1,2], I. Appenzeller[1], S. Noll[3], S. Richling[4], J. Heidt[1], E. Meinköhn[5], and D. Mehlert[2]

[1] Landessternwarte Heidelberg-Königstuhl, D-69117 Heidelberg, Germany
[2] Max-Planck-Institut für Astronomie, Königstuhl 17, D-69117 Heidelberg, Germany
[3] Max-Planck-Institut für extraterrestrische Physik, Giessenbachstr., D-85741 Garching, Germany
[4] Institut d' Astrophysique de Paris, 98bis Bd Arago, 75014 Paris, France
[5] Institut für Theoretische Astrophysik, Albert-Ueberle-Strasse 2, D-69120 Heidelberg, Germany

received; accepted

ABSTRACT

Context. A significant fraction of the high-redshift galaxies show strong Lyα emission lines. For redshifts $z > 5$, most known galaxies belong to this class. However, so far not much is known about the physical structure and nature of these objects.
Aims. Our aim is to analyse the Lyα emission in a sample of high-redshift UV-continuum selected galaxies and to derive the physical conditions that determine the Lyα profile and the line strength.
Methods. VLT/FORS spectra with a resolution of $R \approx 2000$ of 16 galaxies in the redshift range of $z = 2.7$ to 5 are presented. The observed Lyα profiles are compared with theoretical models.
Results. The Lyα lines range from pure absorption (EW = -17 Å) to strong emission (EW = 153 Å). Most Lyα emission lines show an asymmetric profile, and three galaxies have a double-peaked profile. Both types of profiles can be explained by a uniform model consisting of an expanding shell of neutral and ionised hydrogen around a compact starburst region. The broad, blueshifted, low-ionisation interstellar absorption lines indicate a galaxy-scale outflow of the ISM. The strengths of these lines are found to be determined in part by the velocity dispersion of the outflowing medium. We find star-formation rates of these galaxies ranging from $SFR_{\rm UV} = 1.2$ to 63.2 $M_\odot yr^{-1}$ uncorrected for dust absorption.
Conclusions. The Lyα emission strength of our target galaxies is found to be determined by the amount of dust and the kinematics of the outflowing material.

Key words. galaxies: high redshift – galaxies:ISM – galaxies:emission lines

1. Introduction

The 8-10 meter class telescopes and the Hubble Space Telescope have made it feasible to investigate details of the galaxies in the young universe. The majority of the high-redshift galaxies were detected on the basis of their UV colours. Notable examples are the so-called Lyman-break galaxies, which are selected using continuum breaks between 912 and 1216 Å (for a review see Giavalisco 2002). Since a selection by the Lyman break proved to be very efficient in terms of telescope time, a large sample of high-redshift galaxies has been derived. Shapley et al. (2003), e.g., presented the spectra of 798 galaxies at a redshift of ≈ 3. Alternatively, many galaxies, especially in the $z > 5$ universe, have been found by means of their strong Lyα emission (e.g., Hu et al. 2004), the so-called "Lyα emission line galaxies"(LAEs).

Well-defined gaps in the telluric OH-bands allow one to detect LAEs rather efficiently from their excess in narrow-band filters (e.g., Hu et al. 1998; Kudritzki et al. 2000; Rhoads et al. 2000; Maier et al. 2003; Ouchi et al. 2005; Tapken et al. 2006; Nilsson et al. 2006). The frequency and properties of the LAEs have been used to derive the luminosity function (Hu et al. 2004), the star-formation rate in the early universe (Ajiki et al. 2003), the epoch of re-ionisation (Rhoads et al. 2004), and led to the discovery of a large-scale structure at z≈5.7 (Ouchi et al. 2005). Moreover, their luminosity function can be compared to theoretical models (Haiman & Spaans 1999; Thommes & Meisenheimer 2005; Le Delliou et al. 2005), allowing models of galaxy formation and evolution to be constrained. LAEs are the most distant objects in the universe, to have been detected so far (Iye et al. 2006).

Star-forming galaxies produce huge amounts of Lyα photons by recombination in HII regions that are ionised by young stars (e.g., Charlot & Fall 1993). However, the fact that Lyα is a resonance line makes physical interpretation of the Lyα emission challenging. Many theoretical efforts have been made

Send offprint requests to: C. Tapken, Heidelberg (e-mail: tapken@mpia.de)

⋆ Based on observations (proposals: 069.A-0105(A) and 071.A-0307(A)) obtained at the ESO VLT at Cerro Paranal, Chile, and on observations made with HST ACS (GO proposal: 9502).

to treat the radiation transfer of resonance lines, both numerically (e.g., Auer 1968; Adams 1972; Ahn et al. 2001; Richling 2003; Hansen & Oh 2006; Verhamme et al. 2006) and analytically (e.g., Osterbrock 1962; Neufeld 1990). Neutral hydrogen absorbs and re-emits Lyα photons in random directions. As a result the Lyα photons will diffuse in spatial and frequency space (see, e.g., Neufeld 1990). The diffusion in frequency space changes the intrinsic Lyα profile, leading to complex Lyα profile morphologies. The diffusion in space increases the optical path of the Lyα compared to UV-continuum photons. Therefore, any dust distributed uniformly in a neutral medium affects the Lyα photons more strongly than the UV-continuum photons. This could explain the fact that most UV-continuum selected high-redshift galaxies show weak Lyα emission or none at all (Shapley et al. 2003; Noll et al. 2004). As demonstrated by Neufeld (1991) and Hansen & Oh (2006), the spatial distribution of the dust relative to the neutral hydrogen also plays an important role as the Lyα emission can even be less affected by dust than the continuum radiation in a two-phase interstellar medium. Moreover, a large-scale outflow of neutral gas can decrease the number of Lyα resonance scattering (Kunth et al. 1998), if the neutral gas is velocity-shifted with respect to the ionised gas. To conclude, interpretation of the flux, profile, and spatial morphology of the Lyα line is not straightforward. Without further insight into the Lyα emission of star-forming galaxies, the use of LAEs as a tool for constraining models of galaxy formation is limited.

Information about the formation and nature of the Lyα emission in high-redshift galaxies can be derived from the analysis of the UV-restframe continuum, as demonstrated by Shapley et al. (2003). Using average spectra (the so-called composite spectra) of UV-continuum selected high-redshift galaxies, Shapley et al. (2003) and Noll et al. (2004) could show that the strength of the Lyα emission correlates well with other galaxy properties, such as the slope of the continuum or the strength of the interstellar absorption lines. These correlations may be explained by varying amounts of dust and by the kinematics of the host galaxies. Another method for deriving information about the nature of the Lyα emission is to analyse the Lyα profile. Dawson et al. (2002) and Westra et al. (2005) demonstrated that the profile of the Lyα emission can be used to derive properties of the emitting galaxy. The detailed comparison of Lyα profiles with dedicated radiative transfer models can constrain the kinematics of the emitting and neutral ISM. However, the spectra of Shapley et al. (2003) and Noll et al. (2004) had too low a spectral resolution to derive kinematical information from the Lyα profile.

In this paper we analyse a sample of high-redshift UV-continuum selected galaxies in the FORS Deep Field (FDF) to constrain the origin of the Lyα emission, the evolutionary state, and the physical properties of these galaxies. The FORS Deep Field (FDF) is a deep photometric and spectroscopic survey (Appenzeller et al. 2000; Heidt et al. 2003; Noll et al. 2004) carried out with the FORS instruments at the ESO Very Large Telescope (VLT). The analysis of the galaxy sample of this work has made use of the FDF photometric and spectroscopic surveys and the HST-imaging follow-up. In addition R $\approx$ 2000 spectra were obtained, which include the Lyα line. The data are presented in Sect. 2. The properties of the galaxies, including the strength and profile of the Lyα lines, the star-formation rates, and the interstellar absorption lines, are presented in Sect. 3. The Lyα profiles are compared to theoretical models in Sect. 4. The results are discussed in Sect. 5 and the conclusions are given in Sect. 6.

Throughout this paper we adopt $\Omega_\Lambda = 0.7$, $\Omega_M = 0.3$, and $H_0 = 70$ km s^{-1}Mpc^{-1}. The magnitudes are given in the Vega system.

2. Presentation of the data

2.1. Photometric data

The FDF survey consists of deep optical U, B, g, R, I observations obtained with FORS at the VLT and near-infrared J and Ks observations obtained with SofI at the ESO-NTT (Heidt et al. 2003). In addition, deep observations with an SDSS z and a medium-band filter centred at 8350 Å were obtained (Gabasch et al. 2004). The FDF was imaged in the broad-band F814W filter with the Advanced Camera for Surveys (ACS) on the Hubble Space Telescope (HST) in autumn 2002. The field was covered with 4 ACS pointings of 40 minute exposure each, reaching a 10σ limit of 25.6 mag. The data reduction was performed with the standard *CALACS*[1] pipeline, and the combined final mosaic was produced with the multi-drizzle package (Mutchler et al. 2002). The final combined image has a pixel scale of 0.05 arcsec/pixel.

2.2. Target selection for the medium-resolution spectroscopy

The target selection for the medium-resolution spectroscopy was based on the FDF spectroscopic survey (Noll et al. 2004). The FDF spectroscopic survey aimed at obtaining low-resolution spectra (R$\approx$200) of intrinsically bright galaxies with a photometric redshift (Bender et al. 2001; Gabasch et al. 2004) between $z \approx 1$ and 5 with a high signal-to-noise ratio ($\geq$10). Two different selection criteria were applied to select candidates for the medium-resolution spectroscopy from the FDF spectroscopic catalog. First, galaxies with strong Lyα emission were selected. Second, galaxies with bright UV-restframe continuum were added. We included only galaxies whose spectral feature(s) of interest coincide with the wavelength range of the FORS2 grisms 1400V and 1200R and whose expected signal-to-noise ratio was sufficiently high. For the 1400V (1200R) grism, UV-bright continuum galaxies with $z = 2.3 - 3.5$ ($z = 3.0 - 3.5$) and $m_g \leq 24.5$ mag ($m_R \leq 24.5$ mag) were selected. Moreover, galaxies with a Lyα emission strength of $F_{Ly\alpha} \geq 30$ (20) $\times 10^{-21}$Wm^{-2} at $z = 3.0 - 3.5$ ($z = 4.5 - 5$) were included. We also added a few secondary targets selected by their photometric redshifts. Some additional bright objects were included to support the mask positioning during the observation.

[1] www.stsci.edu/hst/acs/analysis

2.3. Observations & data reduction of the medium-resolution sample

The observations were obtained with FORS2 at the VLT UT4 using the holographic grisms 1400V and 1200R. The spectral resolution was R ≈ 2000. The spectral range of the 1400V (1200R) grism was about 4500 to 5800 (5700 to 7300) Å. The central wavelengths depend on the target position in the focal plane. All data were collected in service mode using one single MXU mask for each grism. The FORS2 detector, which consists of two 2k × 4k MIT CCDs, was used in the 100kHz readout mode with high gain. A 2×2 binning was performed during the readout. The observations with the 1400V grism were carried out during August 2002. Eight single exposures with each 47 min integration time were taken, resulting in a total integration time of 6.25 h. The average seeing was 0.81". The observations with the 1200R grism were carried out during July - September 2003. Fourteen single exposures with a total integration time of 10.05 h were obtained. One exposure was excluded from the reduction process, because of moonlight contamination. Therefore, the total effective integration time was 9.45 h. The average seeing was 0.92".

The raw data were reduced using the MIDAS-based FORS pipeline (Noll et al. 2004; Tapken 2005). The two-dimensional spectra were flat-fielded with a dome flatfield and were wavelength-calibrated using calibration spectra of gas discharge lamps. One-dimensional spectra were extracted with a signal-to-noise optimising algorithm (Horne 1986)). A first flux calibration, which included the correction for extinction by the atmosphere, was performed using spectra of standard stars obtained during the same night. The wavelength calibration was verified and, if necessary, corrected by determining the position of sky lines. The one-dimensional spectra were then co-added according to their weighted signal-to-noise. The efficiency of holographic grisms strongly varies with the angle of incidence and thus with the object's position in the telescope's focal plane. Therefore, the low-resolution spectra were used to improve the flux calibration. Some objects were observed only on the medium-resolution spectra. In these cases the varying response function was corrected using the sky spectrum. For this, the sky was extracted from all slits and was divided by the sky in those slits, which had almost the same position as the corresponding slits used in the standard star calibration exposures. In total, 43 objects have been reduced, and six objects were included in both setups. The majority of the 43 objects are galaxies. Only one object is classified as a quasar (QSO Q0103-260 or FDF-4683), and one as a star (FDF-0511). For more information on the 43 objects see Tapken (2005).

3. Results

Since the low-resolution spectra have a broader wavelength range and consequently more spectral features, the redshift for all objects with low-resolution spectra available was taken from the spectroscopic catalog of Noll et al. (2004). FDF-1267 coincided by chance with the slit of a primary target and, therefore, has no corresponding low-resolution spectra. The medium-resolution spectrum shows a strong emission line that has been identified as likely Lyα emission, due to the non-detection of other emission lines and the asymmetric line profile. The redshift of this object is derived from the Lyα emission line. FDF-8304 was selected because its spectral features were expected to coincide with the spectral range of the grism based on the photometric redshift of $z_{\rm phot} = 4.02$. The medium-resolution spectrum shows a Lyα emission line and several low ionisation interstellar absorption lines. In this case again the redshift is derived from the Lyα line.

Thirty galaxies of the medium-resolution sample have a redshift of $z > 2$. Twelve of these 30 galaxies having a sufficiently high continuum SNR for studying their absorption line spectra as discussed in Mehlert et al. (2006). In the present paper the analysis of the medium-resolution spectra is restricted to 16 of the 30 galaxies, where (a) the medium-resolution spectrum contains the Lyα line, either in emission or absorption and where (b) the galaxy is included in the FDF photometric catalog (Heidt et al. 2003). Their redshift, apparent magnitude $m_{\rm R}$, spectral coverage, and average continuum SNR are listed in Table 1. These 16 galaxies are referred to, in the following, as the Lyα medium-resolution sample. This sample covers a redshift range of $z \approx 2.7$ to 5.

In addition to Lyα the galaxies show spectral features such as interstellar absorption lines, stellar wind lines, photospheric lines, and several nebular emission lines. For a detailed discussion of the absorption features, we refer to Mehlert et al. (2006) and Noll et al. (2004). All objects of the Lyα medium-resolution sample, which were included in the FDF spectroscopic survey, are classified as starburst galaxies by Noll et al. (2004), based on the observed UV properties. The spectral energy distribution, the stellar wind lines, and the interstellar absorption line of these objects are typical of starburst galaxies. Furthermore, the line ratio of the nebular lines are typical of starburst galaxies. We could not detect broad lines in either the low-resolution spectra or the medium-resolution spectra, which would indicate AGN activity.

3.1. Observed Lyα line properties

3.1.1. Fluxes and equivalent widths

The Lyα profiles often display both an absorption and an emission component. Only the spectral resolution of the medium-resolution spectra is high enough to separate the two components for each spectrum. We measured the emission line fluxes in the medium-resolution spectra interactively with MIDAS. To calculate the equivalent widths, we estimated the continuum at the wavelength of Lyα from the continuum redwards of the Lyα line. The observed Lyα emission fluxes $F_{\rm Ly\alpha}$ and equivalent widths of the emission component $EW({\rm Ly\alpha_{EM}})$ derived for the Lyα medium-resolution sample are given in Table 2. The error given in Table 2 includes only the contribution of the noise. Any additional error caused by a possibly wrong continuum definition is not included. We also measured the total equivalent widths $EW({\rm Ly\alpha})$, which includes the emission and the absorption component. However, the corresponding measurements are less accurate because of the underlying IGM absorption contributions. In this paper the equivalent width is defined

Table 1. The Lyα medium-resolution sample. The ID corresponds to the catalogs of Heidt et al. (2003) and Noll et al. (2004). The redshift z is from Noll et al. (2004), except for FDF-1267 and FDF-8304, where the redshift is derived from medium-resolution spectra. The 2" aperture magnitude m_R of the galaxies is taken from Heidt et al. (2003). The SNR is the average continuum SNR measured in the complete wavelength range of the spectra. The covered spectral range is given for the restframe of the corresponding galaxies.

ID	z	m_R [mag]	Spectral range 1400V	Spectral range 1200R	SNR 1400V	SNR 1200R
1267	2.788 ± 0.001	27.08 ± 0.07	1158 - 1465	-	0.36	-
1337	3.403 ± 0.004	24.15 ± 0.01	996 - 1261	1235 - 1569	3.53	4.72
2384	3.314 ± 0.004	24.60 ± 0.01	1018 - 1317	1301 - 1643	1.17	3.01
3389	4.583 ± 0.006	25.56 ± 0.02	-	1097 - 1368	-	0.71
4454	3.085 ± 0.004	26.10 ± 0.03	1070 - 1387	-	0.65	-
4691	3.304 ± 0.004	24.79 ± 0.01	1089 - 1393	-	3.78	-
5215	3.148 ± 0.004	24.53 ± 0.01	1062 - 1373	1468 - 1832	3.01	3.98
5550	3.383 ± 0.004	23.95 ± 0.01	1053 - 1351	1315 - 1656	3.78	6.47
5744	3.401 ± 0.003	24.81 ± 0.01	1022 - 1317	-	2.05	-
5812	4.995 ± 0.006	27.55 ± 0.11	-	1040 - 1294	-	0.69
5903	2.774 ± 0.003	23.13 ± 0.01	1181 - 1523	-	12.27	-
6063	3.397 ± 0.004	23.37 ± 0.01	1087 - 1384	1273 - 1609	4.18	5.83
6557	4.682 ± 0.006	25.94 ± 0.02	-	1003 - 1265	-	0.69
7539	3.287 ± 0.003	24.10 ± 0.01	1122 - 1428	1351 - 1698	3.45	4.88
7683	3.781 ± 0.004	24.92 ± 0.01	-	1199 - 1510	-	2.2
8304	4.205 ± 0.003	24.98 ± 0.01	-	1145 - 1433	-	3.37

as positive for emission lines. All equivalent widths are given in the restframe of the corresponding galaxy. Except for FDF-6063, all objects of the medium-resolution sample show a Lyα emission component. FDF-6063 shows only a broad absorption (EW(Lyα) = -17.1 ± 0.9 Å). The measured Lyα fluxes reach up to 186×10^{-21}Wm^{-2}. For strong Lyα emitters, the emission component dominates the total Lyα line. Some galaxies show a strong absorption component and a weak Lyα emission line. The total Lyα emission line is dominated in these cases by the absorption component. An example is FDF-5903 (EW(Lyα) = -12.0 ± 0.5 Å, EW(Lyα_{EM}) = 0.6 ± 0.1 Å). Eight of the 16 galaxies of the medium-resolution sample have total equivalent width EW(Lyα) higher than 20 Å. We also analysed the Lyα emission line of 91 low-resolution spectra of high-redshift galaxies in the FDF spectroscopic catalog. The total Lyα equivalent widths range from absorption (EW(Lyα)≈ -20 Å) to strong emission (EW(Lyα) ≈ 200 Å), while most galaxies have EW(Lyα) of < 20 Å.

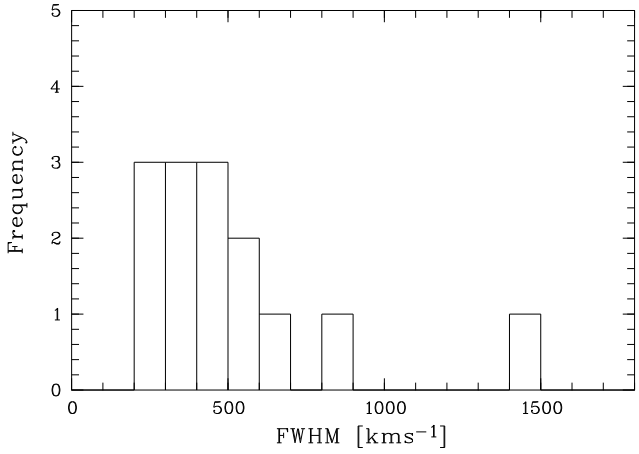

Fig. 2. Distribution of the line widths ($FWHM$) of the Lyα emission line of the medium-resolution sample.

3.1.2. Lyα line profiles

In Fig. 1 all Lyα profiles of the medium-resolution sample are presented. The Lyα profile displays a wide variety of morphologies, from absorption (e.g., FDF-6063), to absorption with a weak emission (FDF-5903), and then to strong emission (e.g., FDF-2384). Most profiles show one asymmetric emission line with a sharp drop on the blue side and a pronounced red wing (e.g., FDF-2384, FDF-5550). This profile type is referred to hereafter as the "asymmetric line profile". FDF-4691, FDF-5215, and FDF-7539 show a secondary emission line blueshifted with respect to the main emission line. This profile type is called "double-peak profile" hereafter.

The full width half maximum (FWHM) values of the Lyα emission lines are listed in Table 2. The distribution of the FWHM values corrected for the instrumental profile is shown in Fig. 2. The observed values range from 200 kms^{-1} up to 1500 kms^{-1}. For FDF-4691 and FDF-7539, this value refers to the envelope of the profile. Most lines have widths below $FWHM$ ≈ 600 kms^{-1}, in agreement with Rhoads et al. (2003), Dawson et al. (2004), and Venemans et al. (2004), who analysed LAEs at a redshift of $z > 5$ and found line widths of $FWHM$ < 500 kms^{-1}.

Figure 3 shows the EW(Lyα) as a function of the line width of the emission line. The values of the line width show a possible anti-correlation with the Lyα equivalent widths. The out-

Table 2. Properties of the Lyα medium-resolution sample. The continuum slope β is taken from Noll et al. (2004). They measured the continuum slope β in the low-resolution spectra of the FDF spectroscopic survey following Leitherer et al. (2002). The Lyα fluxes $F_{\mathrm{Ly}\alpha}$ and equivalent widths EW(Lyα) refer only to the emission component (Sect. 3.1.1). No Lyα emission line was detected in the medium-resolution spectra of FDF-6063. The star-formation rates SFR_{UV} and $SFR_{\mathrm{Ly}\alpha}$ were derived from the UV flux, respectively Lyα flux, using the calibration of Kennicutt (1998) and assuming Case B recombination. The line width $FWHM$(Lyα) refers to the complete profile (Sect 3.1.2) .

ID	z	$SFR_{\mathrm{UV}}[\mathrm{M}_\odot\mathrm{yr}^{-1}]$	β	$F_{\mathrm{Ly}\alpha}[10^{-21}\mathrm{Wm}^{-2}]$	$SFR_{\mathrm{Ly}\alpha}[\mathrm{M}_\odot\mathrm{yr}^{-1}]$	$EW(\mathrm{Ly}\alpha_{\mathrm{EM}})$ [Å]	FWHM(Lyα) [km/s]
1267	2.788 ± 0.001	1.16 ± 0.25	-	25.38 ± 1.30	1.49 ± 0.08	129.8 ± 27.41	235 ± 32
1337	3.403 ± 0.004	27.28 ± 1.15	-2.43	22.09 ± 1.52	2.10 ± 0.14	6.69 ± 0.46	597 ± 84
2384	3.314 ± 0.004	22.74 ± 0.77	-0.55	121.08 ± 3.01	10.8 ± 0.27	83.19 ± 3.89	283 ± 47
3389	4.583 ± 0.006	14.85 ± 2.47	-	46.51 ± 2.23	9.2 ± 0.38	38.82 ± 10.95	354 ± 70
4454	3.085 ± 0.004	1.98 ± 0.49	-2.42	29.91 ± 1.02	2.25 ± 0.08	74.38 ± 11.84	323 ± 47
4691	3.304 ± 0.004	17.88 ± 0.75	-2.46	184.33 ± 1.61	16.31 ± 0.14	79.44 ± 1.61	840 ± 115
5215	3.148 ± 0.004	26.20 ± 0.80	-1.71	121.55 ± 2.63	9.57 ± 0.21	32.48 ± 1.06	483 ± 90
5550	3.383 ± 0.004	44.78 ± 1.07	-1.81	34.89 ± 2.14	3.27 ± 0.2	6.36 ± 0.40	424 ± 85
5744	3.401 ± 0.003	21.23 ± 0.87	-1.02	4.63± 1.06	0.44 ± 0.10	3.30± 0.77	-
5812	4.995 ± 0.006	5.24 ± 0.79	-	40.83 ± 0.78	9.60 ± 0.18	153.8± 26.6	226 ± 23
5903	2.774 ± 0.003	63.14 ± 0.75	-1.15	6.73 ± 1.53	0.39 ± 0.09	0.60 ± 0.14	627 ± 140
6063	3.397 ± 0.004	56.61 ± 1.28	-2.02	-	-	-	-
6557	4.682 ± 0.006	13.85 ± 1.39	-	16.57 ± 0.73	3.35 ± 0.15	30.51 ± 3.04	380 ± 135
7539	3.287 ± 0.003	29.87 ± 0.78	-1.74	28.01 ± 1.84	2.45 ± 0.46	6.84 ± 0.46	1430 ± 230
7683	3.781 ± 0.004	20.40 ± 1.46	-1.16	15.18 ± 1.89	1.85 ± 0.23	9.08 ± 1.16	435 ± 70
8304	4.205 ± 0.003	24.94 ± 5.48	-	5.63 ± 0.74	0.88 ± 0.12	3.21 ± 0.43	500 ± 70

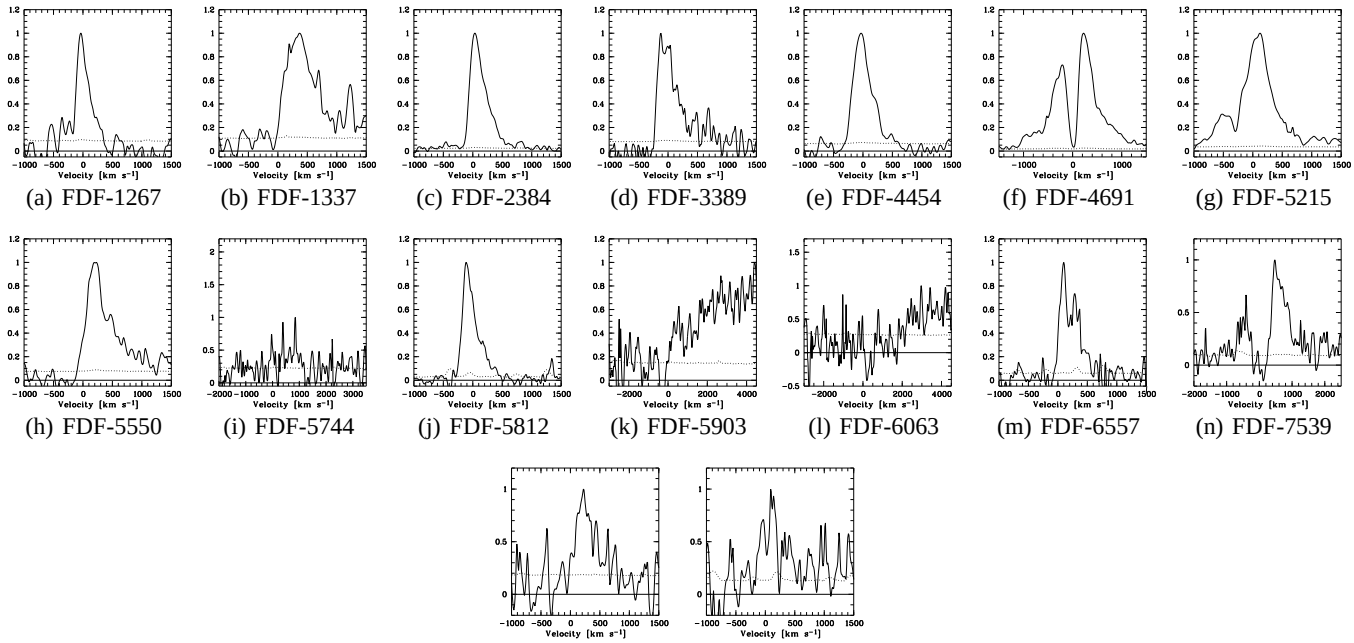

(a) FDF-1267 (b) FDF-1337 (c) FDF-2384 (d) FDF-3389 (e) FDF-4454 (f) FDF-4691 (g) FDF-5215

(h) FDF-5550 (i) FDF-5744 (j) FDF-5812 (k) FDF-5903 (l) FDF-6063 (m) FDF-6557 (n) FDF-7539

(o) FDF-7683 (p) FDF-8304

Fig. 1. The observed medium-resolution spectra of the Lyα line. The abscissa for each figure gives the radial velocity relative to the redshift of the galaxies (see Table 2). The ordinate gives a normalised flux. The dotted line indicates the noise level.

liers with high line width are FDF-4691 and FDF-7539, both galaxies with double-peak profiles.

3.2. Slope of the UV continuum

Studies by, e.g., Calzetti et al. (1994) and Heckman et al. (1998) show that the UV-restframe continuum between 1216 Å and 3000 Å of starburst galaxies can be approximated by $F(\lambda) \approx \lambda^{\beta}$. Noll et al. (2004) measured the slope β for the galaxies in the FDF spectroscopic survey with $2< z <4$ in the range 1200 to 1800 Å, following Leitherer et al. (2002). The values of β for the medium-resolution sample are listed in Table 2. In Fig. 4 the continuum slope β is plotted as a function of the total Lyα equivalent width for the FDF spectroscopic sample β with $2< z <4$. Figure 4 shows that the scatter of the total Lyα equivalent width increases towards steeper slopes.

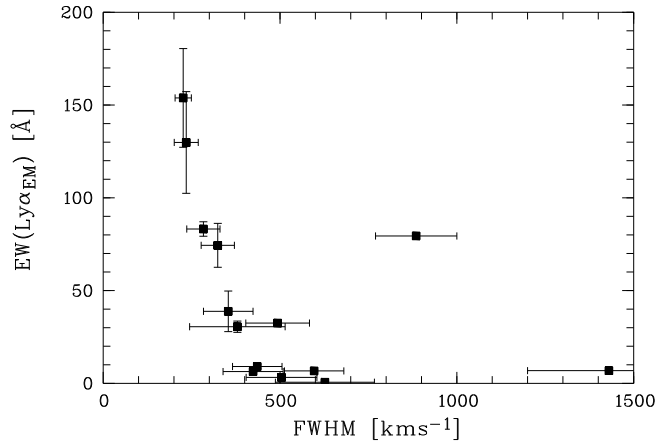

Fig. 3. The Lyα emission line equivalent width as function of the Lyα emission line width.

Galaxies with a continuum slope of β > -2 have Lyα equivalent widths below 25 Å, while galaxies with a blue continuum β < -2 have Lyα equivalent widths in the range of EW(Lyα) = -20 to 100 Å. However, the numbers are too small to derive firm conclusions.

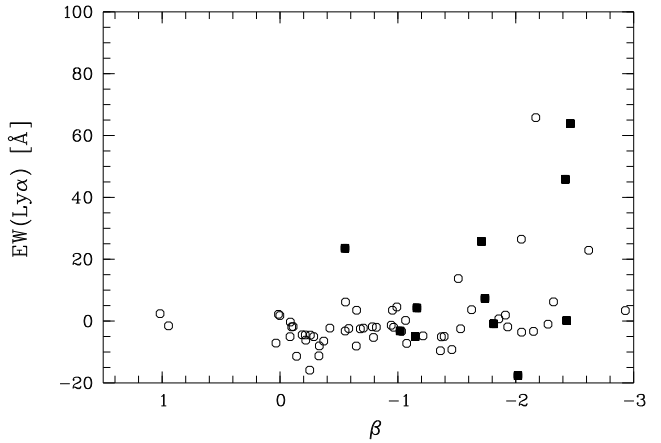

Fig. 4. The total Lyα equivalent width EW(Lyα) vs. the continuum slope β for the FDF spectroscopic sample (circles). Black squares indicate the medium-resolution sample. FDF-4752 is not plotted, since it shows a high equivalent width (EW(Lyα) = 150 Å). FDF-4752 is in the physical vicinity of a QSO (FDF-4683). Therefore, its Lyα emission may be produced differently.

The measured β can be used to derive the dust attenuation for local starburst galaxies (Heckmann et al. 1998). Since the intrinsic slope depends only weakly on metallicity and starburst age for a continuous starburst (and an instantaneous starburst within the first 20 Myrs), the observed slope is determined essentially by the amount of dust (Heckmann et al. 1998; Leitherer et al. 1999). However, the relation of the attenuation and β depends on the physical properties of the ISM and dust in the galaxy. Therefore, this relationship can be ambiguous (Noll & Pierini 2005).

3.3. Interstellar absorption lines

The equivalent widths of the prominent interstellar SiII λ1261, OI/SiII λ1303, and CII λ1335 absorption lines were measured for galaxies in the medium-resolution sample. We restricted ourselves to these three lines, because the spectral coverage of the medium-resolution spectra was limited. Only seven galaxies had a continuum SNR that was high enough to determine the interstellar absorption lines in detail. The equivalent widths of the three lines are given in Table 3. The equivalent widths of the interstellar absorption lines range between -1.1 Å and -3.6 Å, in good agreement with previous studies (e.g., Noll et al. 2004). Moreover, the line widths of the interstellar absorption lines were measured in the medium-resolution spectra. Only the mean of the lines SiII λ1260 and CII λ1335 are included in Table 3. SiII/OI λ1303 was excluded, because the two lines cannot be separated. The line widths range between 350 and 770 kms^{-1}. These broad line widths are typical for high-redshift galaxies. For their sample of about 800 spectra of high-redshift galaxies Shapley et al. (2003) found an average velocity dispersion for the low-ionisation interstellar absorption lines of $FWHM_{\rm LIS}$ = 560 ± 150 kms^{-1}.

Velocity offsets of the interstellar absorption lines with respect to the Lyα emission were derived, using the redshift of the Lyα emission component as a reference. For these measurements, the OI/SiII λ1303 blend was again excluded. The galaxies show a negative velocity offset between the Lyα emission line and the interstellar absorption lines (see Table 3), indicating either a redshifted Lyα emission or blue-shifted interstellar absorption lines, or a combination of both. The mean velocity offset is ≈ -580 kms^{-1}, in good agreement with the values found in other studies (e.g., Shapley et al. 2003). If we assume that the redshifts of Noll et al. (2004) represent the systemic redshift of the objects, we derive a mean velocity offset of the interstellar absorption lines of ≈ -150 kms^{-1}. Therefore, the Lyα emission would be redshifted by ≈ 430 kms^{-1}, if the Noll et al. (2004) measurements indeed represent the systemic redshift. Adelberger et al. (2003) find for a sample of high-redshift galaxies that the Lyα emission is redshifted by 310 kms^{-1} with respect to the optical nebular emission lines, while the low-ionisation interstellar absorption are blueshifted by -150 kms^{-1}.

In Fig. 5 the mean equivalent widths of the interstellar absorption lines SiII λ1261 and CII λ1335 are plotted as a function of the mean line widths. A correlation is indicated in Fig. 5. The strength of the saturated ISM absorption lines does not strongly depend on the column density, but on the covering fraction and on the velocity dispersion of the ISM (Shapley et al. 2003). The covering fraction of the low-ionisation interstellar absorption lines can be measured by the observed residual intensities at the line position, and the velocity dispersion by the line width. While the correlation in Fig. 5 suggests a significant influence of the gas kinematics, the scatter indicates that the covering fraction also plays a role. The galaxies for which the EW(LIS) and $FWHM$(LIS) could be measured

have a lower average Lyα equivalent width (average EW(Lyα) = -3.2 Å) than the full medium-resolution sample (average EW(Lyα) = 37 Å). This is caused by the fact that the galaxies with lower observed Lyα equivalent width have a brighter UV continuum in the FDF spectroscopic survey (see also Table 3 in Shapley et al. 2003). It remains unclear whether the tentative correlation found above also applies to galaxies with strong Lyα emission.

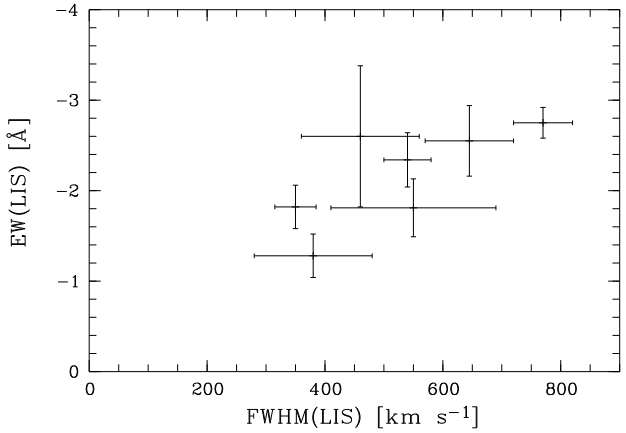

Fig. 5. The equivalent width of the interstellar absorption lines plotted as a function of the line width of the interstellar absorption lines.

3.4. Morphology

In Fig. 6 we show HST/ACS F814W images of galaxies of the Lyα medium-resolution sample. Since the HST/ACS image covers only the central part of the FDF field, not all the galaxies were imaged. The HST/ACS images show the rest-frame UV of the starburst galaxies, which is dominated by the young stars. Moreover, as the surface brightness scales with $(z+1)^{-4}$, the extended regions of the galaxies are not easily detected. The observed diameters of the objects are of the order of $\approx$ 2 kpc, which is typical of Lyman-break galaxies at a redshift of three (Ferguson et al. 2004). The strong Lyα emitters appear compact (e.g., FDF-4691 or FDF-5215), while the galaxies with a weak (or no) Lyα emission line are elongated and irregular (e.g., FDF-5903 and FDF-6063). We detected neither (strong) spatial extension of the Lyα emissions in the two-dimensional spectra nor a spatial offset between the Lyα emission and the continuum for all of the members of the medium-resolution sample, excepting FDF-2384. Figure 6b shows that FDF-2384 has two components, a compact one and a diffuse component, north east of the compact component. The two-dimensional spectrum shows that the continuum is emitted by the compact object, while the Lyα emission is emitted by the diffuse object.

3.5. Star-formation rates

Using the flux of the Lyα lines, we computed the star-formation rates for the medium-resolution and low-resolution samples. The line luminosities were derived by assuming an isotropic emission and Case B recombination, where the medium was assumed to be optically thick for all Lyman continuum and Lyman line photons. In this case approximately 2/3 of all recombinations lead to Lyα emission (Osterbrock 1989). To derive the star-formation rates, the calibration of Kennicutt (1998) was used. The derived star-formation rates $SFR_{\mathrm{Ly}\alpha}$ for the medium-resolution sample are given in Table 2.

The star-formation rates were also estimated from the UV spectral fluxes, which have been measured in the low-resolution spectra (if available, otherwise measured in the medium-resolution spectra). Again, the calibration of Kennicutt (1998) was used. The resulting star-formation rates SFR_{UV} range between 1.16 $M_{\odot}yr^{-1}$and 64 $M_{\odot}yr^{-1}$(Table 2). No correction for dust absorption was applied to these star-formation rate values. As shown by Table 2 the star-formation rates derived from the Lyα line are on average lower than the star-formation rates derived from the UV continuum. For the medium-resolution Lyα sample, we find a ratio of $SFR_{\mathrm{Ly}\alpha}$ / $SFR_{\mathrm{UV}} \approx 0.2$. Although the conversion of luminosities to star-formation rates are subject to systematic uncertainties, for most galaxies it can be concluded that the Lyα emission is lower than expected from the star-formation rate derived by the UV continuum. This agrees with other measurments of star-formation rates derived from the Lyα flux and UV spectral flux (Ajiki et al. 2003).

4. The Lyα profile

To constrain the physical properties of the Lyα emitting regions of the galaxies, we compared three of our observed Lyα profiles with calculated model profiles using the finite element line formation code of Richling and Meinköhn (Richling & Meinköhn, 2001; Meinköhn & Richling 2002). The code is particularly well-suited to calculating the radiative transfer in a non-static scattering medium. However, the code in its present form is not suitable for high optical depths. Therefore, we restricted the finite element modelling to the double-peaked profiles of FDF-4691, FDF-5215, and FDF-7539. A spherical two-component model with a central line emission region surrounded by a shell of neutral HI gas was assumed. For the emission from the central region, we assumed a Gaussian emission profile. The model is mainly characterised by the velocity dispersion of the intrinsic emission line, as well as the velocity dispersion, the neutral column density, and the outflow velocity of the shell. The exact geometrical properties of the model are of minor importance for the computed line profiles (Richling et al. 2007). In Fig. 4 the comparison of the Lyα profiles of FDF-5215 and FDF-7539 is shown with the theoretical model. The results for FDF-4691 have already been described by Tapken et al. (2004). The derived fit parameters are listed for the three galaxies in Table 4. While N_{HI} could not be constrained well for FDF-4691, an upper limit can be found for FDF-5215: N_{HI} cannot exceed $N_{\mathrm{HI}} = 2 \times 10^{16}$ cm^{-2}.

FDF-4691, FDF-5215, and FDF-7539 have been modelled with finite element calculations as well as with Gaussian emission and Voigt absorption components. Both approaches assume a central emission region producing a Gaussian emission

Table 3. Equivalent widths of the prominent interstellar absorption lines. The equivalent widths were measured in the medium-resolution spectra, except EW(OI/SiII λ1303) and EW(CII λ1335) for FDF-5744, which were measured in the low-resolution spectra. The velocity offset δv between the Lyα line and the prominent low-ionisation interstellar absorption lines and the widths $FWHM$(LIS) of the interstellar absorption lines are also included. The average values for SiII λ1261 and CII λ1335 are given.

ID	EW(SiII λ1261) [Å]	EW(OI/SiII λ1303) [Å]	EW(CII λ1335) [Å]	$FWHM$(LIS) [kms^{-1}]	δv [kms^{-1}]
1337	- 2.03 ± 0.42	- 1.68 ± 0.4	- 1.62 ± 0.25	350 ± 35	-607 ± 45
5550	- 2.61 ± 0.27	- 2.95 ± 0.70	- 2.07 ± 0.55	540 ± 40	-620 ± 85
5744	-2.62 ± 0.43	-2.61 ± 1.1	-2.57 ± 1.52	460 ± 100	-560 ± 120
5903	-2.54 ± 0.26	-3.53 ± 0.29	-2.96 ± 0.22	770 ± 50	-760 ± 80
6063	-2.52 ± 0.59	-2.84 ± 0.65	-2.57 ± 0.66	645 ± 75	-
7539	-1.4 ± 0.34	-1.14 ± 0.3	-1.17 ± 0.35	380 ± 100	-80 ± 30
8304	-1.81 ± 0.32	-1.83 ± 0.38	-2.53 ± 0.44	550 ± 140	-860 ± 140

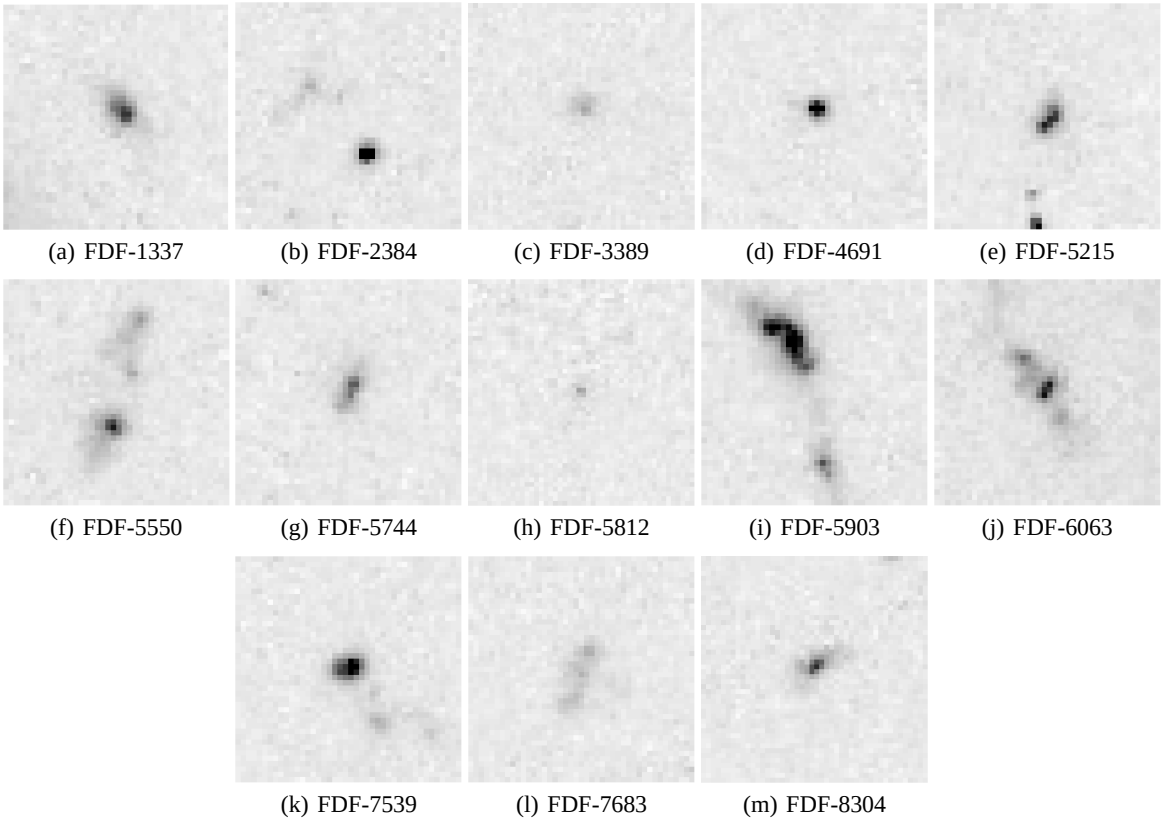

(a) FDF-1337 (b) FDF-2384 (c) FDF-3389 (d) FDF-4691 (e) FDF-5215

(f) FDF-5550 (g) FDF-5744 (h) FDF-5812 (i) FDF-5903 (j) FDF-6063

(k) FDF-7539 (l) FDF-7683 (m) FDF-8304

Fig. 6. HST/ACS images of the sample of medium-resolution galaxies. Each image is 15 × 15 kpc large, north is up, east is left.

Table 4. The derived fit parameters of the finite-element calculations. The velocity dispersion of the emission region v_{dis}(core), the velocity dispersion of the shell, the HI column density of the shell N_{HI}, and the outflow velocity of the shell are given.

ID	v_{dis}(core) [kms^{-1}]	v_{dis}(shell) [kms^{-1}]	N_{HI} [cm^{-2}]	$v_{outflow}$ [kms^{-1}]
4691	600	60	4×10^{17}	12
5215	500	125	$< 2 \times 10^{16}$	125
7539	1140	190	2.5×10^{16}	190

profile. But the models differ with respect to the radiative transfer in the absorption component. The absorption component of the finite element calculations re-emits the photons. The re-emitted photons are redistributed in frequency space, leading, e.g, to two emission peaks. The model with Gauss emission and Voigt absorption assumes that all absorbed photons are lost. They are either absorbed by dust or absorbed by extended neutral clouds, which distribute the photons in physical space and therefore have surface brightnesses that are too low to be detected (Kunth et al. 1998). The assumption that all absorbed photons are lost may not be valid for high-redshift galaxies, where the absorbing HI region is compact with respect to the slit width, and the dust content within the HI region is expected to be low. The line fitting of the Lyα absorption component using Voigt absorption profiles will lead to an underestimate of

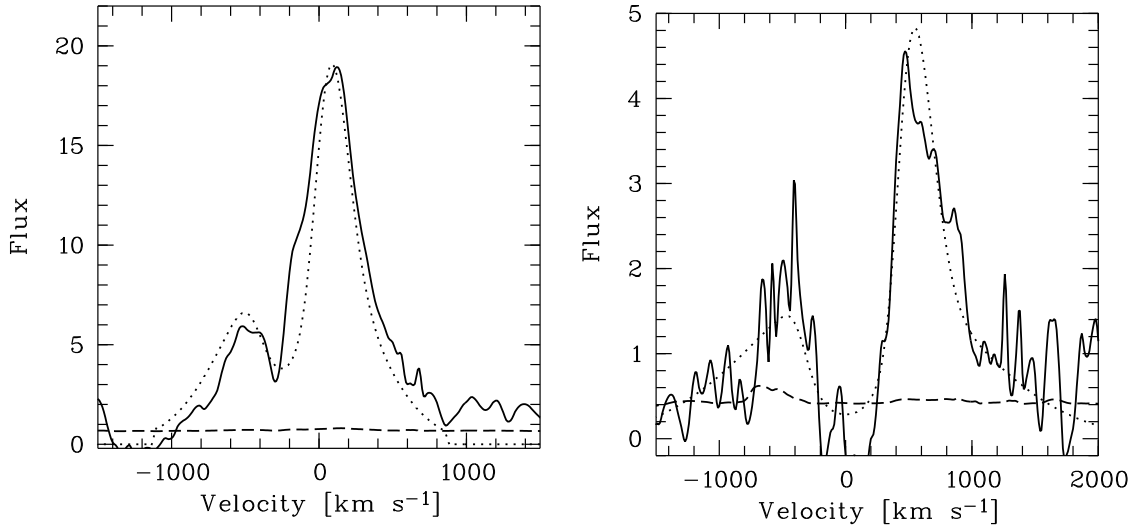

(a) FDF-5215 (b) FDF-7539

Fig. 7. Comparison of the observed Lyα lines (solid line) of FDF-5215 and FDF-7539 and the best-fit theoretical models (dotted line). The dashed line indicates the noise level of the observed spectrum.

the true hydrogen column density (see also Verhamme et al. 2006).

5. Discussion

5.1. Lyα profiles

Meinköhn & Richling (2002) and Ahn et al. (2003) modelled Lyα profiles assuming an expanding neutral shell surrounding the Lyα emission region. If the shell is static, the profile shows two emission peaks with the same flux, blueshifted and redshifted with respect to the systemic redshift. The flux of the blue peak is decreased, if the expansion velocity is increased. If the expansion velocity is sufficiently high, the blueshifted secondary peak disappears. Ahn et al. (2003), Ahn (2004), and Verhamme et al. (2006) show, that the red wing of the Lyα profile gets more flux. This is caused by Lyα photons, which are backscattered from the far side (from an observers point of view) of the expanding shell, which recedes from an observer. In this case an asymmetric profile is observed, which can show a secondary emission component redshifted with respect to the main emission component. Therefore, the model of an expanding neutral shell surrounding a Lyα emitting region can quantitativly reproduce the asymmetric profiles (see also Dawson et al. 2002) and the symmetric profiles. A parameter that determines the morphology of the emission profile is the expansion velocity of the neutral shell. By a given neutral column density and velocity dispersion of the neutral shell, a low expansion velocity will lead to a double-peaked Lyα profile, while a higher expansion velocity would lead to an asymmetric profile. The fact that asymmetric profiles in most cases are observed seems to indicate that the galaxies show an outflow of interstellar HI. At a redshift of $z = 3$ the mean transmission of the IGM is $T = 0.7$ (Songaila 2004). Therefore, we expect that the observed fraction of double-peak profiles at a redshift of $z = 3$ is not significantly changed by absorption of the blue part of the profile of the IGM. Most profiles of Lyα emission lines in the literature are asymmetric. However, double-peaked profiles are only observable if the signal-to-noise ratio and the spectral resolution of the spectrum is sufficiently high. A significant number of spectra with high SNR and resolution have only been observed for LAEs at $z > 5$, where the absorption of the intergalactic medium is severe ($T < 0.2$, Songaila 2004). At this redshift a double-peak profile would not be observed, since the blue peak would be absorped by the IGM. So far, double-peaked Lyα profiles have been observed only at redshift $z \approx 3$ (Fosbury et al. 2003; Christensen et al. 2004; Venemans et al. 2005).

5.2. The origin of the strength of the Lyα emission in high-redshift galaxies

We find no indication of AGN activity in our sample (Sect. 3). In the following we assume that the Lyα emission lines are caused by starburst activity. In principle, other mechanisms are also possible. However, since the UV continuum is caused by an ongoing (or recent) starburst, starburst activity is a reasonable explanation for the observed Lyα fluxes. The intrinsic total Lyα equivalent width EW(Lyα) can be predicted using stellar population synthesis models if one assumes that the Lyα photons are produced by recombination in HII regions ionised by young stars. The intrinsic total Lyα equivalent width EW(Lyα) also includes the contribution by stars and supernovae remnants. For very young ($\approx$ 2 Myr) and very low metallicity ($< 4 \times 10^{-4}$ Z$_\odot$) starburst galaxies, the Lyα equivalent width can reach up to 1500 Å (Schaerer 2003). Star-forming galaxies with moderate age (>10 Myr) and metallicity and a initial mass function (IMF) in the range of values observed in the local

universe have a predicted EW(Lyα) in the range of 50 to 200 Å (Charlot & Fall 1993). However, for certain star-formation histories, the total Lyα line can even be observed in absorption (Charlot & Fall 1993). The majority of ionising photons are produced by early O main-sequence stars, which have a lifetime less than 4 Myrs. Stars with lifetimes greater than 10 Myrs do not produce significant amounts of hydrogen ionising photons. If O stars are absent, the intrinsic Lyα flux is very low making the Lyα equivalent width small. While a continuous starburst leads to high (> 100 Å) intrinsic Lyα equivalent widths, as long as the starburst lasts (Leitherer et al. 1999; Leitherer et al. 2001), an exponential decaying star-formation rate (time scale 10 Myrs; Charlot & Fall 1993) leads to small equivalent widths after several 10 Myrs.

Most observed total Lyα equivalent widths are lower than 20 Å (Sect. 3.1; see also, e.g, Shapley et al. 2003; Noll et al. 2004). Several effects could lead to a low observed Lyα equivalent width: (a) a suitable epoch of the star-formation history, where the O stars have already left the main sequence the observed epoch, while B and A stars producing a strong UV-continuum are still present, (b) orientation effects resulting in the escape of the Lyα photons in a different direction, and (c) absorption of the Lyα photons by dust and neutral hydrogen (Chen & Neufeld 1994). In the following we discuss these three effects.

Shapley et al. (2003) and Noll et al. (2004) present composite spectra of high-redshift galaxies. Both present composite spectra, which were produced by certain types of high-redshift galaxies, including galaxies with small observed Lyα equivalent width. Strong stellar wind lines are visible in the composite spectra of galaxies with small Lyα equivalent width (Shapley et al. 2003; Noll et al. 2004). For example, the CIV $\lambda\lambda$ 1548, 1551 line of the composite spectrum of the Lyα subsample group 3 (EW(Lyα) = -1 Å) of Shapley et al. (2003) displays a P Cygni profile. Only in the observed UV-restframe spectra of early O main-sequence stars and supergiant OB stars does the CIV line show a P Cygni profile (Walborn & Panek 1984; Walborn & Nichols-Bohlin 1987). It is possible that we observe the galaxies with low Lyα emission in a short period of their star formation history (SFH), when the main sequence O stars, which produce most ionising photons, are no longer present, and only massive supergiants are present. However, it appears unlikely that the majority of the high-redshift galaxies with small Lyα equivalent widths are in this phase of their SFH. In addition, Noll et al. (2004) find a strong increase of the strength of the Lyα emission from $z \approx 2.3$ to $z \approx 3.2$. There is no reason for the galaxies at a redshift of $z \approx 3.2$ still to be forming stars, but the galaxies at $z \approx 2.3$ just turned off their star-formation. Therefore, we conclude that an SFH, where the young OB stars are absent but enough B and A stars produce a strong UV continuum, cannot explain the low observed Lyα fluxes easily. However, one needs multi-wavelength data to derive the intrinsic Lyα flux in detail (for a discussion of the determination of the intrinsic Lyα flux, see Schaerer & Pello 2005). Therefore, we cannot rule out that some of the observed variety of the Lyα emission in high-redshift galaxies is caused by a different intrinsic Lyα strength.

Another explanation for the observed small Lyα equivalent widths can be an orientation effect. In this case the Lyα photons are produced in huge numbers and escape the galaxy but are emitted in a direction not coinciding with the line of sight to us. As discussed by Charlot & Fall (1993) and Chen & Neufeld (1994), a certain geometric configuration could lead to an anisotropic emission of the Lyα photons. The strength of the Lyα line depends on the angle at which we observe the galaxy. Although such orientations effects may play a role for individual galaxies, the observed correlation between the Lyα equivalent widths and the strength of the interstellar low-ionisation lines (discussed below) cannot be explained if orientation effects are the only reason for the small Lyα equivalent widths.

Since the special stellar population and orientations effects provide no plausible explanation for the small observed Lyα equivalent widths, we conclude, that the most reasonable explanation for the variation in the observed Lyα equivalent widths is the combined effect of dust absorption and resonance scattering of Lyα photons in neutral hydrogen, enriched with dust (Charlot & Fall 1993; Chen & Neufeld 1994). As pointed out by Chen & Neufeld (1994), this mechanism can also explain the strong Lyα absorption seen in many high-redshift galaxies, since the combined effect of dust absorption and resonance scattering also affects the stellar continuum. The absorption of the Lyα photons depends on the total amount of dust, the neutral gas, the spatial distributation of the dust relative to the gas, and the kinematical properties. If no neutral gas is present, Lyα photons and UV-continuum photons are affected by the same amount of dust.

The analysis of composite spectra of high-redshift galaxies shows the importance of the ISM for the strength of the Lyα emission: Shapley et al. (2003) and Noll et al. (2004) find a strong anti-correlation between the equivalent width of Lyα EW(Lyα) and the equivalent width of the low-ionisation metallic interstellar absorption lines EW(LIS). In Lyman-break galaxies the latter are blueshifted with respect to the system velocity, which is explained by a galaxy-wide outflow, the superwind (Adelberger et al. 2003; Shapley et al. 2003). Observations of Lyman-break galaxies favours a scenario where clouds of cold neutral gas (which are traced by the low-ionisation lines) are embedded in hot, ionised gas (Shapley et al. 2003). The star-formation activity accelerates the cold gas outwards. The cold neutral gas phase of the superwind influences the intrinsic Lyα emission line strongly (see also Ferrara & Ricotti 2006 for a model for gas outflow that explains the observed properties of Lyman-break galaxies, including the strengths of their Lyα emission). The properties of the superwind will determine the observed Lyα flux. One can describe this superwind by the following model parameters: the velocity dispersion b, the neutral column density of the hydrogen $N_{\rm HI}$, the mean outflow velocity v, and the spatial covering fraction. Concerning the radiative transfer, the superwind is rather similar to the expanding shell model used by us in Sect. 5.1 to simulate the formation of the observed Lyα profiles. Therefore, the agreement of the observed and computed profiles can also be regarded as support of the superwind model. In principle, the observed properties of the superwind (like the mean outflow velocity) can be used to constrain the parameters of the expanding

shell model, which decribes the Lyα profiles (Verhamme et al. 2006). This will hopefully help for understanding the observed properties of the Lyα emission in more detail.

6. Conclusions

We analysed a sample of 16 restframe UV-continuum selected $2.7 < z < 5$ galaxies using medium-resolution FORS2 spectra. The Lyα lines range from pure absorption (EW(Lyα) = -17 Å) to strong emission (EW(Lyα) = 153 Å). Most of the Lyα lines show an asymmetric profile, with a sharp drop on the blue side and an extended red wing. Three Lyα lines display a double-peaked profile with two separate emission lines. The profiles were compared to calculated profiles computed by a radiative transfer code. Both types of profiles, the asymmetric and the double-peaked profiles, can be explained by a uniform model of an expanding shell of neutral hydrogen surrounding a compact starburst region (see also Ahn et al. 2001, 2003). One parameter, which determines the morphology of the profile, is the expansion velocity of the neutral shell. A low expansion velocity leads to a double-peaked Lyα profile, while a higher expansion velocity would lead to an asymmetric profile. The Lyα emission strengths of our target galaxies are found to be determined by the amount of dust and the kinematics of the outflowing material. Broad, blueshifted, low-ionisation interstellar absorption lines were detected. They indicate a galaxy-scale outflow of the ISM. The strengths of these ISM lines were found to be partly determined by the velocity dispersion of the outflowing medium.

Acknowledgements. Our research has been supported by the German Science Foundation DFG (SFB 439). We thank Daniel Schaerer, Anne Verhamme, and Klaus Meisenheimer for valuable discussions. We would also like to thank the referee for his/her insightful comments that improved the paper. We thank the Paranal staff for having carried out the service mode observations and Maurilio Pannella for providing the HST images.

References

Adams, T. F. 1972, ApJ, 174, 439
Adelberger, K. L., Steidel, C. C., Shapley, A. E., & Pettini, M. 2003, ApJ, 584, 45
Ahn, S. 2004, ApJL, 601, L25
Ahn, S., Lee, H., & Lee, H. M. 2001, ApJ, 554, 604
—. 2003, MNRAS, 340, 863
Ajiki, M., Taniguchi, Y., Fujita, S. S., et al. 2003, AJ, 126, 2091
Appenzeller, I., Bender, R., Böhm, A., et al. 2000, The Messenger, 100, 44
Auer, L. H. 1968, ApJ, 153, 783
Bender, R., Appenzeller, I., Böhm, A., et al. 2001, in Deep Fields: Proceedings of the ESO Workshop Held at Garching, Germany, 9-12 October 2000, ESO ASTROPHYSICS SYMPOSIA. Edited by S. Cristiani, A. Renzini, and R.E. Williams. Springer-Verlag, 2001, p. 96
Calzetti, D., Kinney, A. L., & Storchi-Bergmann, T. 1994, ApJ, 429, 582
Charlot, S., & Fall, S. M. 1993, ApJ, 415, 580
Chen, W. L., & Neufeld, D. A. 1994, ApJ, 432, 567
Christensen, L., Sánchez, S. F., Jahnke, K., et al. 2004, A&A, 417, 487
Dawson, S., Spinrad, H., Stern, D., et al. 2002, ApJ, 570, 92
Dawson, S., Rhoads, J. E., Malhotra, S., et al. 2004, ApJ, 617, 707
Ferrara, A., & Ricotti, M. 2006, MNRAS, 373, 571
Fosbury, R. A. E., Villar-Martín, M., Humphrey, A., et al. 2003, ApJ, 596, 797
Gabasch, A., Bender, R., Seitz, S., et al. 2004, ApJ, 421, 41
Giavalisco, M. 2002, ARA&A, 40, 579
Haiman, Z., & Spaans, M. 1999, ApJ, 518, 138
Hansen, M.,& Oh, S. P. 2006, MNRAS, 367, 979
Heckman, T. M., Robert, C., Leitherer, C., Garnett, D. R., & van der Rydt, F. 1998, ApJ, 503, 646
Heidt, J., Appenzeller, I., Gabasch, A., et al. 2003, A&A, 398, 49
Horne, K. 1986, PASP, 98, 609
Hu, E. M., Cowie, L. L., McMahon, R. G. 1998, ApJL, 502, L99
Hu, E. M., Cowie, L. L., Capak, P., et al. 2004, AJ, 127, 563
Iye, M., Ota, K., Kashikawa, N., et al. 2006, Nature, 446, 186
Kennicutt, R. C. 1998, ARA&A, 36, 189
Kudritzki, R.-P., Méndez, R. H., Feldmeier, J. J., et al. 2000, ApJ, 536, 19
Kunth, D., Mas-Hesse, J. M., Terlevich, E., et al. 1998, A&A, 334, 11
Le Delliou, M., Lacey, C., Baugh, C. M., et al. 2005, MNRAS, 357, 979
Leitherer, C., Schaerer, D., Goldader, J. D., et al. 1999, ApJS, 123, 3
Leitherer, C., Leão, J. R. S., Heckman, T. M., et al. 2001, ApJ, 550, 724
Leitherer, C., Calzetti, D., & Martins, L. P. 2002, ApJS, 574, 114
Maier, C., Meisenheimer, K., Thommes, E., et al. 2003, A&A, 402, 79
Malhotra, S., & Rhoads, J. E. 2002, ApJL, 565, L71
Mehlert, D., Tapken, C., Appenzeller, I., et al. 2006, A&A, 455, 835
Meinköhn, E., & Richling, S. 2002, A&A, 392, 827
Mutchler, M., Koekemoer, A. M., & Hack, W. 2002, in The 2002 HST Calibration Workshop, 70
Neufeld, D. A. 1990, ApJ, 350, 216
—. 1991, ApJL, 370, L85
Nilsson, K.,K., Fynbo, J., P., U., Moller, P., & Orsi, A. 2006, astro-ph/0611239
Noll, S., Mehlert, D., Appenzeller, I., et al. 2004, A&A, 418, 885
Noll, S., & Pierini, D. 2005 A&A, 444, 137
Osterbrock, D. E. 1962, ApJ, 135, 195
—. 1989, Astrophysics of gaseous nebulae and active galactic nuclei (Research supported by the University of California, John Simon Guggenheim Memorial Foundation, University of Minnesota, et al. Mill Valley, CA, University Science Books, 1989, 422 p.)
Ouchi, M., Shimasaku, K., Akiyama, M., et al. 2005, ApJ, 620, 1
Rhoads, J. E., Malhotra, S., Dey, A., et al. 2000, ApJ, 545, 85
Rhoads, J. E., Dey, A., Malhotra, S., et al. 2003, AJ, 125, 1006
Rhoads, J. E., Xu, C., Dawson, S., et al. 2004, ApJ, 611, 59
Richling, S., Meinköhn, E., Kryzhevoi, N., & Kanschat, G. 2001, A&A, 380, 776
Richling, S. 2003, MNRAS, 344, 553
Richling, S., Hippelein, H., Meisenheimer, K., & Tapken, C. 2007, A&A submitted.
Schaerer, D. 2003, A&A, 397, 527
Schaerer, D., & Pello, R. 2005, MNRAS, 362, 1054
Shapley, A. E., Steidel, C. C., Pettini, M., & Adelberger, K. L. 2003, ApJ, 588, 65
Songaila, A. 2004, AJ, 127, 2538
Taniguchi, Y., Shioya, Y., Masaru, A., et al. 2003, JKAS, 36, 22
Tapken, C., Appenzeller, I., Mehlert, D., Noll, S., & Richling, S. 2004, A&A, 416, L1
Tapken, C. 2005, Doctoral Thesis, Universität Heidelberg
Tapken, C., Appenzeller, I., Gabasch, A., et al. 2006, A&A, 455, 145
Thommes, E., & Meisenheimer, K. 2005, A&A, 430, 877

Venemans, B. P., Röttgering, H. J. A., Overzier, R. A., et al. 2004, A&A, 424, L17
Venemans, B. P., Röttgering, H. J. A., Miley, G. K., et al. 2005, A&A, 431, 793
Verhamme, A., Schaerer, D., & Maselli, A. 2006, A&A submitted
Walborn, N. R., & Panek, R. J. 1984, ApJL, 280, L27
Walborn, N. R., & Nichols-Bohlin, J. 1987, PASP, 99, 40
Westra, E., Jones, D. H., Heath, D., et al. 2005, A&A, 430, L21